Journal of Materials Chemistry B

PAPER

Check for updates

Simultaneous antioxidant and neuroprotective effects of two-dimensional (2D) MXene-loaded isoquercetin for ischemic stroke treatment†

Limin Fan,‡[ac] Xinhua Lin,‡[a] Limin Hong,‡[a] Lehui Li,[a] Run Lin,[a] Tianbin Ren,[c] Jia Tian*[b] and Miao Chen [ID] *[a]

Oxidative stress and reactive oxygen species drive ischemic stroke and its related complications. New antioxidant medications are therefore crucial for treating ischemic stroke. We developed Ti$_2$C@BSA-ISO nanocomposites loaded with the hydrophobic drug isoquercetin (ISO) encapsulated in BSA on Ti$_2$C nano-enzymes as a novel therapeutic nanomedicine for the treatment of ischemic stroke targeting reactive oxygen species (ROS). TEM visually proved the successful preparation of Ti$_2$C@BSA-ISO, and the FTIR, XPS, zeta potential and DLS together demonstrated the acquisition of Ti$_2$C@BSA-ISO. In addition, the enzyme-mimicking activity of Ti$_2$C was evaluated and the antioxidant capacity of Ti$_2$C@BSA-ISO was verified. Ti$_2$C@BSA-ISO was able to reverse the decrease in cellular activity caused by ROS. Experiments *in vivo* showed that Ti$_2$C@BSA-ISO could promote neuroprotection and scavenging of ROS in the hippocampal CA1 area and cerebral cortex of rats, thereby inhibiting cellular death and alleviating ischaemic stroke. Specifically, Ti$_2$C@BSA-ISO alleviated ischemic stroke by inhibiting NLRP3/caspase-1/GSDMD pathway-mediated pyroptosis. Our study demonstrates the effectiveness of nanomedicines that can be directly used as drugs for the treatment of ischemic stroke in synergy with other drugs, which greatly expands the application of nanomaterials in the treatment of ischemic stroke.

1. Introduction

Stroke is the primary global cause of behavioral disorders[1,2] causing clinical and economic burdens due to neuronal death post-stroke.[3] After cerebral ischemia, neurons experience an ischemic cascade resulting in necrotic or apoptotic cell death associated with hypoxia, excitotoxicity, and oxidative stress.[4] Currently, there is no viable medical approach to restore impaired brain function.[5] Thus, reducing ischemia–reperfusion injury is crucial.[6]

Ischemia damages mitochondria and causes inflammation, leading to neuronal cell death.[6–11] Dysregulation during reperfusion disrupts antioxidant balance, causing ROS accumulation, inflammation, and brain injury.[12] Endogenous antioxidants work well under normal conditions but are insufficient under pathological conditions.[13,14] Researchers are exploring nanomaterials that mimic natural antioxidants to protect damaged neurons caused by a lack of oxygen. These materials are stable, have a wide range of antioxidant properties, and are efficient at eliminating harmful free radicals.[15] Cerium dioxide nanoparticles show promise for treating ischemic stroke,[16] but their toxicity[17–19] and ability to cross the blood–brain barrier[20–25] must be addressed before clinical use. More research is needed to understand the link between nanoenzymes and ischemic stroke pathogenesis, as well as their ability to target cerebral ischemic sites and reduce side effects in normal tissues. Thus, designing effective antioxidant and anti-inflammatory strategies for ischemic stroke treatment remains a great challenge.[25]

Two-dimensional nanomaterials, a new subtype of nanomaterials with ultrathin layered topology, are increasingly garnering interest in biomedical applications due to their high specific surface area and outstanding physicochemical properties.[13,26–29] Two-dimensional materials have a large "materials library" that provides a wealth of options for meeting the various requirements for nanocarriers in biomedical applications.[30] The discovery of graphene has led to the rapid development of 2D materials. Presently, graphene and GO have been known to be used as a carrier for drug delivery, gene

a Department of Emergency, The First Affiliated Hospital of Hainan Medical University, No. 31, Longhua Road, Longhua District, Haikou City, Hainan Province, 570102, P. R. China. E-mail: marcy_cm@hainmc.edu.cn

b Intensive Medical Unit, Hainan General Hospital, Hainan Affiliated Hospital of Hainan Medical University, No. 19 Xiuhua Road, Haikou, China. E-mail: 5298439@qq.com

c School of Medicine, Tongji University, Shanghai 200092, P. R. China

† Electronic supplementary information (ESI) available. See DOI: https://doi.org/10.1039/d3tb01973j

‡ These authors contributed equally to this work.

This journal is © The Royal Society of Chemistry 2024

J. Mater. Chem. B, 2024, **12**, 2795–2806 | 2795

therapy, bioimaging, biosensors, and antibacterial composites and as a scaffold for cell culture in tissue engineering.[31–34] In addition, MXene 2D materials have received increasing attention for their antioxidant properties due to their tunable elemental valence states, in addition to their ability to act as drug carriers.[35] Among them, 2D Ti_2C MXene with reactive oxygen scavenging activity shows good chemical responsiveness to ROS, exhibits intrinsic characteristics of ROS-responsive biodegradation, and degrades to safe Ti(II) or Ti(III) after treatment, or even TiO_2.[36–39] Thus, Ti_2C MXene would be an effective antioxidant with broad-spectrum ROS scavenging ability and biosafety for the treatment of ischemic stroke.

However, the development of ischemic stroke is a dynamic process. Rapid progression in early ischemia, where revascularization and antioxidation are crucial to treatment, and neuro-restoration in late ischemia is another key to treatment.[16] Isoquercitrin (ISO), a natural flavon, is considered a potent radical scavenger. It has various physiological properties such as antioxidant, anti-inflammatory and antiviral, and has protective effects on multiple organs such as heart, liver, skin, lung, kidney, and nervous system. Studies have shown that ISO can reduce ischemic reperfusion injury in the heart, kidney, and brain, tissues.[40,41] Thus, ISO and its derivatives may achieve both antioxidant and neuroprotection, essential for treating and protecting stroke.
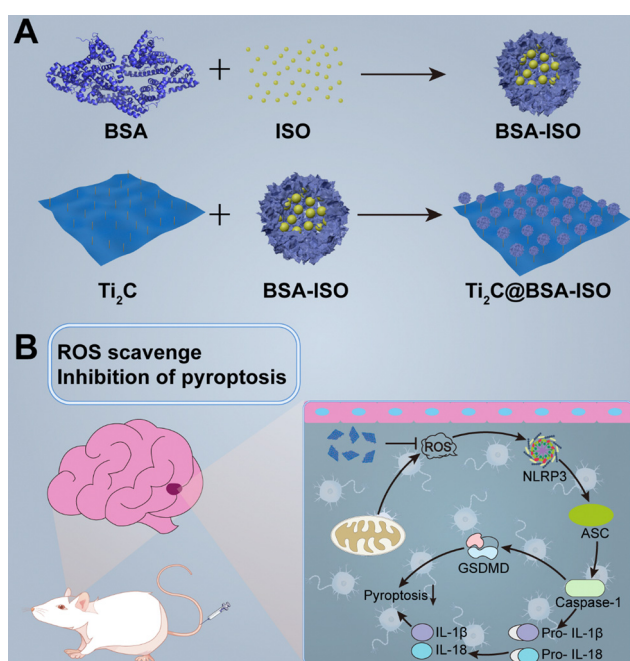
This study reports a successful paradigm of simultaneous antioxidant and neuroprotection in ischemic stroke by 2D Ti_2C nanoenzymes combined with the therapeutic drug isoquercetin (Scheme 1). A nanoformulation ($Ti_2C@BSA-ISO$) for ischemic stroke therapy was successfully prepared by loading the hydrophobic drug isoquercetin (ISO) encapsulated within BSA on

Ti_2C nanoenzyme, which has strong free radical scavenging ability. Ti_2C exerts mimetic enzymatic activity and actively scavenges ROS at the focal site; isoquercetin promotes angiogenesis, neurogenesis, and neuroplasticity in the ischemic area of the brain, which has a neuroprotective effect in ischemic stroke. In a rat model of middle cerebral artery occlusion (MCAO), $ISO@BSA-Ti_2C$ showed excellent ROS scavenging ability and reduced cerebral infarction and cerebral edema; meanwhile, it effectively inhibited neuroinflammation and neuronal damage by inhibiting the NLRP3/caspase-1/GSDMD-mediated pyroptosis pathway. $Ti_2C@BSA-ISO$ combines antioxidant and neuroprotective abilities and provides a new avenue for treating ischemic stroke.
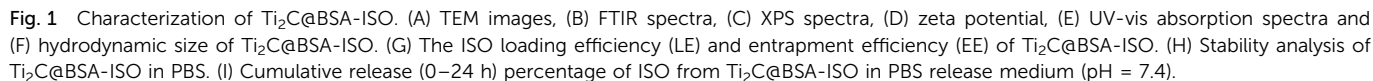
2. Results

2.1 Synthesis and characterization of $Ti_2C@BSA-ISO$

Stable $Ti_2C@BSA-ISO$ nanoparticles were prepared by self-assembling activated BSA with ISO molecules. Disulfide bonds were first disrupted and then re-formed. An amide bond was formed between the carboxyl group of Ti_2C and the amino group of BSA. BSA-ISO was confirmed to be bonded to the lamellar structure of Ti_2C by TEM, indicating successful preparation of $Ti_2C@BSA-ISO$ (Fig. 1A). The Fourier transform infrared (FTIR) spectra of Ti_2C, BSA, ISO, BSA@ISO and $Ti_2C@BSA-ISO$ are shown in Fig. 1B. BSA@ISO showed a vibrational absorption peak of –OH near 3403 cm^{-1}, and a series of absorption peaks between 3010 and 2500 cm^{-1} are attributed to the telescopic vibration peaks of BSA and ISO alkane C–H and olefin C=CH, which increase in the peak intensity due to the reaction of BSA with ISO; furthermore, its absorption peak at 1656 cm^{-1} is a composite of the BSA amide I band and the ISO –C=O–, and the absorption peaks at 1497 cm^{-1} and 1464 cm^{-1} were the bending vibration peaks of ISO benzene ring, which indicated that BSA@ISO was successfully constructed. Compared with the FTIR spectra of BSA@ISO, the absorption peak of $Ti_2C@BSA-ISO$ at 3389 cm^{-1} is attributed to the stretching vibration of –OH, and a series of absorption peaks between 3014 and 2500 cm^{-1} are the stretching vibration peaks of alkane C–H and olefin C=CH, which are enhanced by the introduction of Ti_2C. The absorption peak at 1650 cm^{-1} is the vibrational absorption peak of the amide bond formed by the reaction of Ti_2C with BSA, and the bending vibrational peaks attributed to the ISO benzene ring appear near 1495 cm^{-1} and 1464 cm^{-1}. At the same position of the Ti 2p XPS peak of Ti_2C, $Ti_2C@BSA-ISO$ showed Ti 2p XPS peaks, indicating the successful construction of $Ti_2C@BSA-ISO$ (Fig. 1C). In addition, the binding energies of 283.8 eV and 285.2 eV of C1s in $Ti_2C@BSA-ISO$ are attributed to C=C and C=O, respectively. The binding energies of 400.9 eV and 398.8 eV N 1s are attributed to C–N and C–NH$_2$, respectively. The O 1s spectrum of $Ti_2C@BSA-ISO$ shows the presence of oxygen-containing groups at 531.5 eV and 532.8 eV, which are attributed to the oxygen atoms in the C=O and C–O. The spectra of Ti 2p shows the peaks of Ti–C at 457.6 eV and

Scheme 1 Schematic of synthesis and mechanism for improving ischemic stroke of the $Ti_2C@BSA-ISO$.

2796 | J. Mater. Chem. B, 2024, **12**, 2795–2806

This journal is © The Royal Society of Chemistry 2024

Fig. 1 Characterization of Ti$_2$C@BSA-ISO. (A) TEM images, (B) FTIR spectra, (C) XPS spectra, (D) zeta potential, (E) UV-vis absorption spectra and (F) hydrodynamic size of Ti$_2$C@BSA-ISO. (G) The ISO loading efficiency (LE) and entrapment efficiency (EE) of Ti$_2$C@BSA-ISO. (H) Stability analysis of Ti$_2$C@BSA-ISO in PBS. (I) Cumulative release (0–24 h) percentage of ISO from Ti$_2$C@BSA-ISO in PBS release medium (pH = 7.4).

462.4 eV, which implies that there is Ti^{+2} in Ti$_2$C@BSA-ISO, and the other two peaks (458.2 eV and 463.6 eV) are attributed to Ti–O. Both BSA-ISO and Ti$_2$C were negatively charged with zeta potentials of −13.53 mV and −19.8 mV, respectively. The zeta potential was reduced to −23.67 mV after BSA-ISO was bound to Ti$_2$C by covalent interaction (Fig. 1D). Fig. 1E shows distinct

characteristic ISO peaks at 255 nm and 350 nm, indicating successful binding of ISO to BSA-ISO and Ti$_2$C@BSA-ISO. The particle size was measured by dynamic light scattering (DLS) with ~229.8 nm of the obtained Ti$_2$C@BSA-ISO (Fig. 1F). All these results indicated the successful preparation of Ti$_2$C@BSA-ISO. Quantitative analysis showed that the ISO loading

This journal is © The Royal Society of Chemistry 2024

J. Mater. Chem. B, 2024, **12**, 2795–2806 | **2797**

efficiency (LE) and entrapment efficiency (EE) of Ti$_2$C@BSA-ISO were ~38.7% and ~84.9%, respectively (Fig. 1G). Fig. 1H shows that Ti$_2$C@BSA-ISO was stable in 10% FBS medium for 48 hours with no significant change in the nanoparticle size. In addition, the results of ISO release in PBS buffer (pH = 7.4) at 37 °C are shown in Fig. 1I. The cumulative ISO release was elevated during the first 10 hours, steadily increased during the next 15 hours, and eventually leveled off. These drug release data suggested that Ti$_2$C@BSA-ISO has an excellent release behavior, with 75% ISO release within 10 h, suggesting that Ti$_2$C@BSA-ISO can act *in vivo* in a short period.

2.2 Enzyme-mimicking activities of Ti$_2$C for ROS scavenging

To evaluate the enzyme-like properties of Ti$_2$C in scavenging ROS, we used the TAC method to measure its antioxidant capacity. As demonstrated in Fig. 2A, Ti$_2$C's antioxidant capacity increased significantly with concentration, confirming its excellent properties. Subsequently, the various mimetic enzyme (SOD, CAT, and GPx) activities of Ti$_2$C were assessed. O$_2^{\bullet-}$ is the main component of ROS. SOD catalyzes toxic O$_2^{\bullet-}$ into H$_2$O$_2$ and O$_2$ to protect cells from high levels of oxidative stress. The SOD-like activity of Ti$_2$C was assessed by inhibiting the product (formazan, 450 nm) of the reaction of WST-1 with O$_2^{\bullet-}$. Ti$_2$C catalytically reduced the amount of O$_2^{\bullet-}$, thereby inhibiting the formazan production. As the concentration of Ti$_2$C increased, the amount of formazan decreased, indicating the SOD-like activity of Ti$_2$C (Fig. 2B). H$_2$O$_2$ is a major ROS, and CAT can decompose it into H$_2$O and O$_2$, avoiding excessive accumulation and alleviating oxidative stress. Ti$_2$C demonstrated CAT-like activity by generating O$_2$ from H$_2$O$_2$. A large

number of bubbles containing O$_2$ were observed as Ti$_2$C was incubated with H$_2$O$_2$, and the production of O$_2$ increased over time (Fig. 2C), providing direct evidence of the CAT-like activity of Ti$_2$C. In cells, GPx is crucial for reducing H$_2$O$_2$ levels. To do this, GPx employs intracellular GSH to catalyze the conversion of H$_2$O$_2$ to H$_2$O and GSSG, which is then converted back to GSH by glutathione reductase (GR) and NADPH. We investigated the GPx-like activity of Ti$_2$C using the GR-coupling method. This method involves monitoring the decrease in NADPH concentration spectrophotometrically at 340 nm. The absorbance of NADPH decreased as the Ti$_2$C concentration increased, as shown in Fig. 2D. In summary, Ti$_2$C has multiple enzyme-like activities which can scavenge ROS effectively.

2.3 The antioxidant ability of Ti$_2$C@BSA-ISO *in vitro*

To confirm the applicability of the antioxidant capacity of Ti$_2$C@BSA-ISO for ischemic stroke, the intrinsic cytotoxicity of Ti$_2$C@BSA-ISO was investigated. During two days of co-incubation with SH-SY5Y cells, Ti$_2$C@BSA-ISO below 75 μg mL^{-1} showed good biocompatibility. Therefore, the antioxidation of Ti$_2$C@BSA-ISO was further investigated *in vitro*. Besides, SH-SY5Y cells were treated with the Fenton reagent and H$_2$O$_2$, which can lead to high intracellular production of ROS. The CCK-8 kit and the DCFH-DA probe were used to examine the protective effect against oxidative stress-induced cell death. Positive controls for free radicals were SH-SY5Y cells treated with the Fenton reagent and H$_2$O$_2$. The Ti$_2$C@BSA-ISO group showed higher cell viability and decreased fluorescence intensity compared to the control group, indicating increased ROS scavenging activity (Fig. 3A–D). Reversal of cell death by
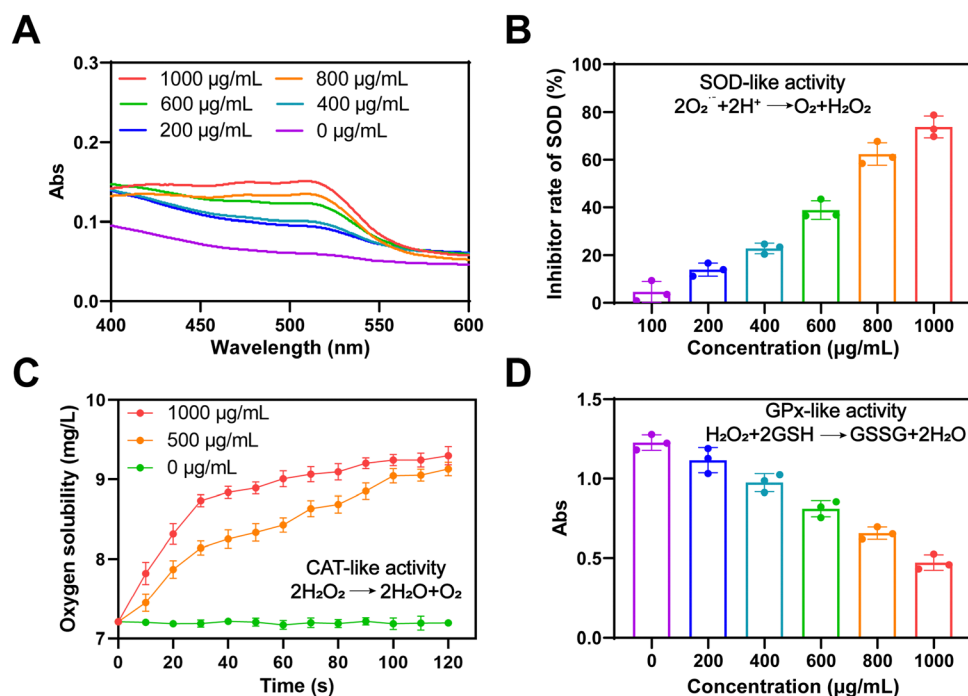

Fig. 2 Enzyme-mimicking activities of Ti$_2$C for ROS scavenging. (A) Total antioxidant capacity of Ti$_2$C. (B) The SOD-mimicking activity of Ti$_2$C. (C) The CAT-mimicking activity of Ti$_2$C. (D) The GPx-mimicking activity of Ti$_2$C.
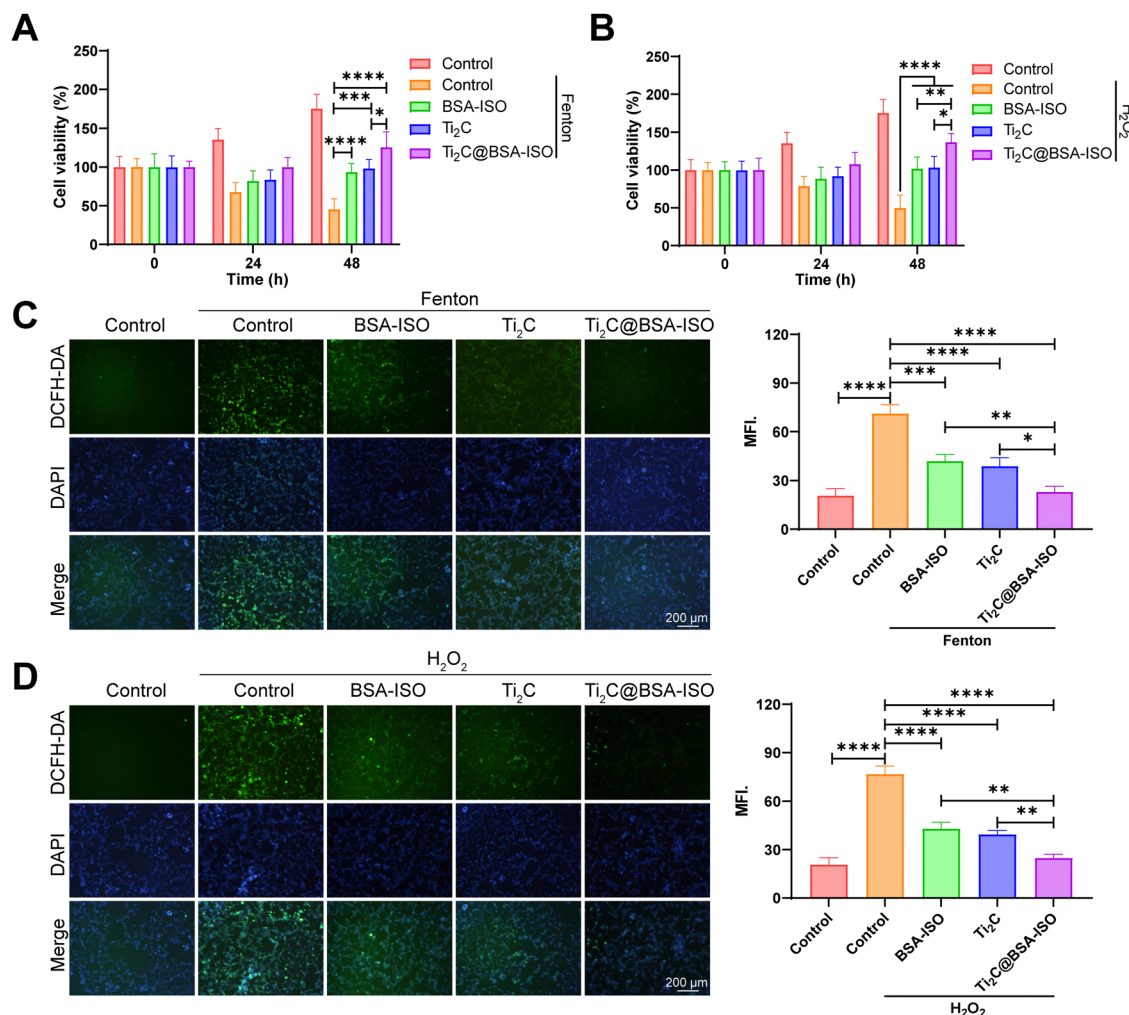
2798 | *J. Mater. Chem. B*, 2024, **12**, 2795–2806

This journal is © The Royal Society of Chemistry 2024

Fig. 3 The antioxidant ability of Ti$_2$C@BSA-ISO *in vitro*. The cell viability of Ti$_2$C@BSA-ISO on the Fenton reagent (A) and H$_2$O$_2$ (B) treated SH-SY5Y cells. The ROS levels of Ti$_2$C@BSA-ISO on the Fenton reagent (C) and H$_2$O$_2$ (D) treated SH-SY5Y cells.

Ti$_2$C@BSA-ISO *via* antioxidation is similar to previously reported results.[24,42,43]

2.4 The therapeutic effect of Ti$_2$C@BSA-ISO *in vitro*

To investigate the potential effect of Ti$_2$C@BSA-ISO on neuron survival and function during ischemic stroke, we first constructed an OGD/R cell model *in vitro*. Primary cortical neurons were maintained under oxygen-glucose deprivation (OGD) for 4 h, followed by re-oxygenation (OGD/R) for the applied time. According to the CCK-8 results in Fig. 4A, cell viability with OGD/R treatment was declined. Ti$_2$C@BSA-ISO administration significantly improved the survival of the modeling cells. The live/dead staining also demonstrated the protective effect of Ti$_2$C@BSA-ISO (Fig. 4B). OGD/R-treated primary cortical neurons showed the most significant proportion of dead cells. After co-incubation with Ti$_2$C@BSA-ISO, the red fluorescence (dead cells) of the primary cortical neurons was significantly reduced, implying that Ti$_2$C@BSA-ISO improved the survival of the neuronal cells. To clarify the cellular uptake of Ti$_2$C@BSA-ISO, co-localization experiments of FITC-labelled Ti$_2$C@BSA-ISO and

primary cortical neurons were performed (Fig. 4C). Fluorescence images showed that FITC-labelled Ti$_2$C@BSA-ISO localized within primary cortical neurons and that the fluorescence increased with time (Fig. 4D), demonstrating that Ti$_2$C@BSA-ISO could be taken up intracellularly by the cells.

2.5 The therapeutic effect of Ti$_2$C@BSA-ISO *in vivo*

To confirm the therapeutic effect of Ti$_2$C@BSA-ISO *in vivo*, we further investigated its ameliorative effect in a rat model of ischemic stroke induced by 90-minute middle cerebral artery occlusion (MCAO) surgery. TTC staining was used to visually determine the effect of Ti$_2$C@BSA-ISO on the cerebral infarct volume (Fig. 5A and B). The brain tissues of normal control rats were uniformly pale red with no brain infarct lesions; MCAO-induced animals showed a significant increase in infarct volume, and the brain infarct sites in the group were stained white. ISO and BSA-ISO treatments reduced the infarct volume to some extent, and the effect was more pronounced in the Ti$_2$C@BSA-ISO treatment group. The reduction of cerebral infarcts was associated with improved neurological scores in
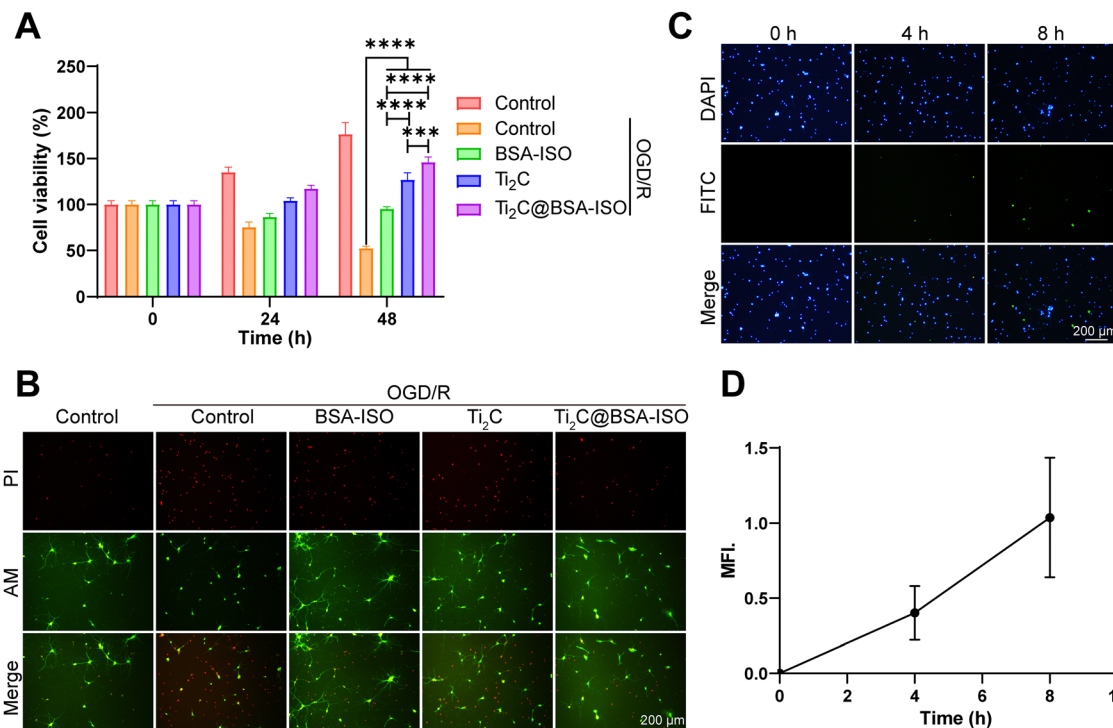
This journal is © The Royal Society of Chemistry 2024

J. Mater. Chem. B, 2024, **12**, 2795–2806 | **2799**

Fig. 4 The therapeutic effects of Ti$_2$C@BSA-ISO *in vitro*. (A) The cell viability of primary hippocampal neurons treated with different treatment groups for 0 h, 24 h, and 48 h. (B) The live/dead staining of primary cortical neurons with varying treatment groups was evaluated by the calcein-AM/PI kit. (C) and (D) The uptake of Ti$_2$C@BSA-ISO by primary cortical neurons after 0 h, 4 h, and 8 h co-incubation.

mice, and neurological tests were used to evaluate the neurological prognosis of Ti$_2$C@BSA-ISO – treated rats. The results showed that the neurological scores of the Ti$_2$C@BSA-ISO – treated MCAO group were significantly higher than those of other treated groups and just lower than those of normal rats, suggesting that Ti$_2$C@BSA-ISO treatment could improve neurological deficits (Fig. 5C).

Then, Nissl staining was used to label the hippocampal CA1 region and cortical neurons of Nissl bodies to evaluate the neuronal damage after MCAO. In the normal control group, the hippocampal CA1 region and cortical neurons were morphologically entire, and dark blue Nissl bodies were visible in the cytoplasm. After MCAO, hippocampal CA1 region and cortical neurons were wrinkled and deformed, and damaged neurons were not selectively stained due to cell membrane disruption. In the ISO-treated group, the hippocampal CA1 region and cortical neurons were partially restored, and after treatment with BSA-ISO only, the hippocampal CA1 region and cortical well-formed neurons. In the Ti$_2$C@BSA-ISO group, the neuroprotective effect was more apparent, and most of the neuronal cells in the hippocampal CA1 region and cortex remained intact. The above results indicated that T Ti$_2$C@BSA-ISO could attenuate neuronal damage in the CA1 region of the hippocampus and cortex after MCAO (Fig. 5D).

In addition, TUNEL staining further assessed the apoptosis and loss of neurons in the hippocampal CA1 area and cortex. The control group had good neuronal morphology in the hippocampal CA1 region and showed no significant neuronal

apoptosis (Fig. 5E and F). In contrast, the number of Tunel-positive neurons significantly increased after MCAO, indicating neuronal loss. Apoptotic neurons were reduced after ISO or BSA-ISO treatment. However, Ti$_2$C@BSA-ISO treatment significantly reduced apoptotic neurons in the hippocampal CA1 region and rescued neurons to a great extent. The results in the cerebral cortex were similar, and apoptosis was significantly inhibited by ISO and BSA-ISO treatment (Fig. 5G and H). These results suggest that ISO and BSA-ISO have good anti-apoptotic effects on neurons in the MCAO rat model.

2.6 Ti$_2$C@BSA-ISO alleviated the ischemic stroke by suppression of the NLRP3/caspase-1/GSDMD pathway-mediated pyroptosis

Inflammation and pyroptosis play a role in the damage caused by stroke.[44,45] Pyroptosis is a type of programmed cell death that involves the inflammasome, cell membrane openings, and the release of IL-1β and IL-18 controlled by GSDM proteins.[46,47] The NLRP3 inflammasome is made up of NLRP3, ASC and caspase-1 protein making it one of the most important inflammasomes.[48] Bacterial and internal factors activate the NLRP3 inflammasome, which then increases the levels of NLRP3 and pro IL 1β. Immune cells recruit pro-caspase-1 *via* ASC, which activates and converts pro-IL-1β and pro-IL-18 into active forms.[49] Caspase-1 cleaves GSDMD to form pore-forming fragments, which causes cell swelling and rupture, releasing inflammatory factors IL-1β and IL-18, leading to an inflammatory response and pyroptosis. The NLRP3/caspase-1/GSDMD
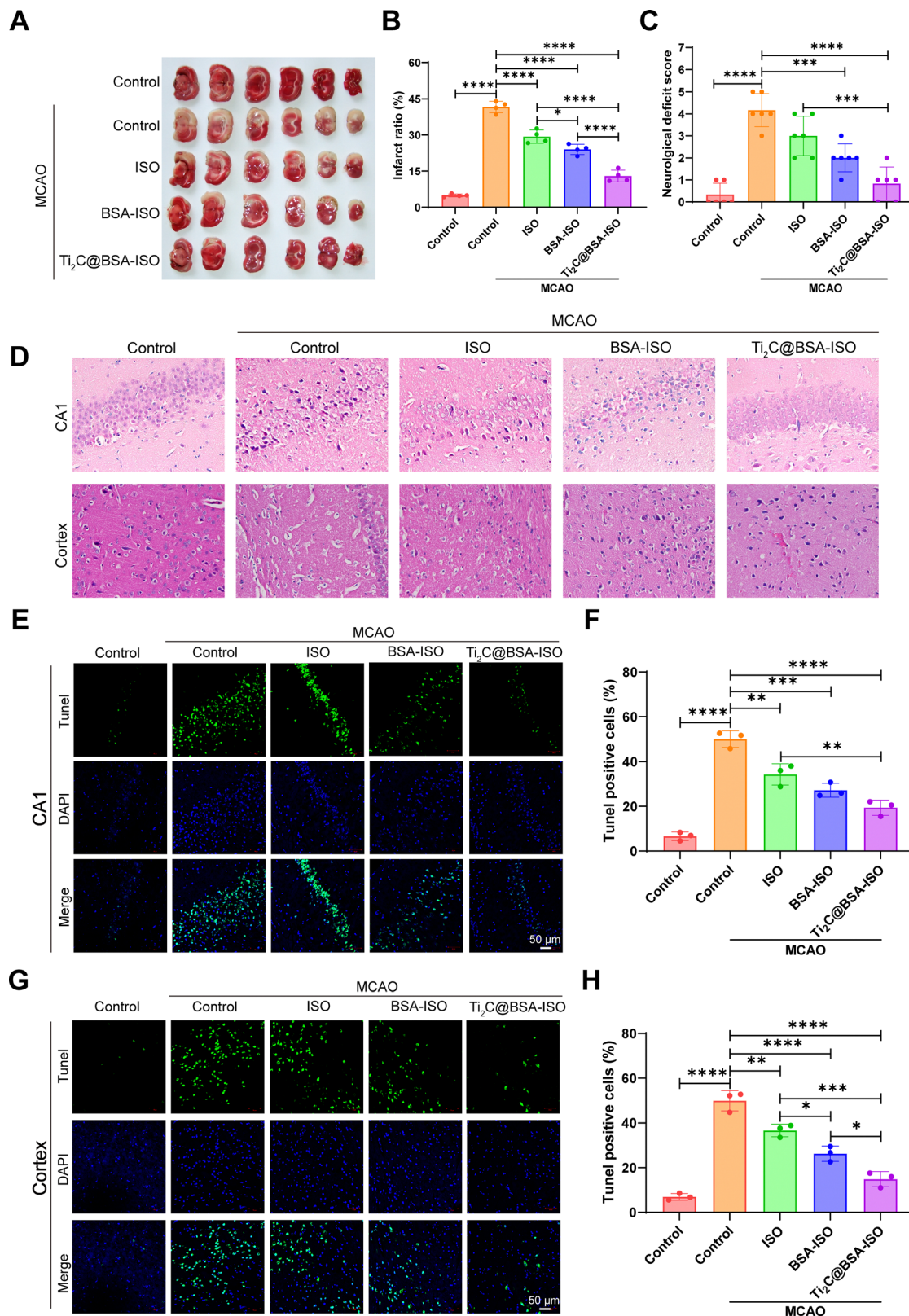
Fig. 5 The therapeutic effect of Ti$_2$C@BSA-ISO *in vivo*. (A) Representative images of TTC-stained coronal brain sections of rats after MCAO and (B) analysis of the percentage of infarct volume in each group. (C) Neurological tests with Ti$_2$C@BSA-ISO treatment of rats after MCAO. (D) Neurons in the CA1 region of the hippocampus and cerebral cortex were observed using Nissl staining. (E) The labeling technique used tunnel staining (green) to identify cells in the CA1 region of the hippocampus while nuclei were labeled with DAPI in blue. (F) The graph presenting the statistical analysis results showing the percentage of Tunel cells found in the CA1 region of the hippocampus. (G) Tunnel labeling (green) was employed for cells in the cortex whereas DAPI staining was utilized to label nuclei (blue). (H) Statistical analysis determined the percentage of Tunel cells in the cortex.
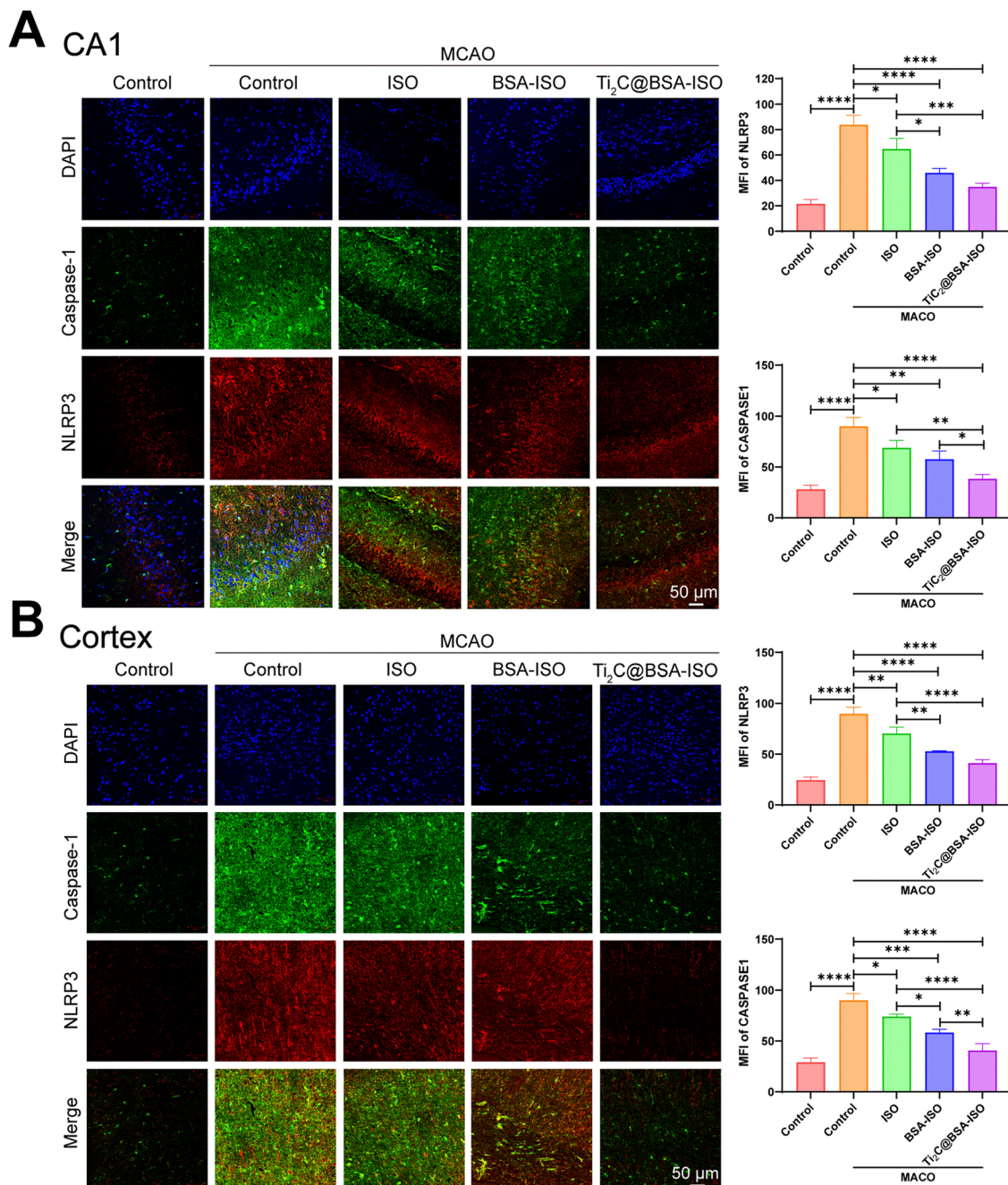
Fig. 6 Ti$_2$C@BSA-ISO inhibits microglia inflammation. Representative images of co-immunostaining of caspase-1 (green) and NLRP3 (red) and quantitation of caspase-1 and NLRP3 positive microglia in (A) the hippocampal CA1 region and (B) the cerebral cortex.

pathway regulates pyroptosis, dominated by NLRP3 activation, but ROS can also activate it.[50–52] Inflammation in the brain after a stroke is linked to NLRP3 inflammasome-mediated microglia pyroptosis and functional recovery.[53,54] Thus, inhibiting inflammatory vesicle-dependent microglial pyroptosis may ameliorate ischemic brain injury.

Pro-inflammatory pyroptosis in the ischemic brain is mainly mediated by microglia.[55] To investigate whether MCAO triggers pyroptosis in microglia within the hippocampal CA1 region and cerebral cortex of rats, we employed immunofluorescence

staining and western blotting techniques to assess the levels of markers associated with microglia. The immunofluorescence staining (Fig. 6A and B) showed a higher number of caspase-1 and NLRP3 positive cells in the hippocampal CA1 region and cerebral cortex of rats with MCAO compared to the control group. Additionally, the western blot analysis revealed increased levels of NLRP3, ASC, cleaved caspase 1, GSDMD-N, and IL-1β expression in the hippocampal CA1 region and cerebral cortex of rats after MCAO (Fig. 7A and B, Fig. S1, ESI†). These findings provide supporting evidence for pyroptosis occurrence in the
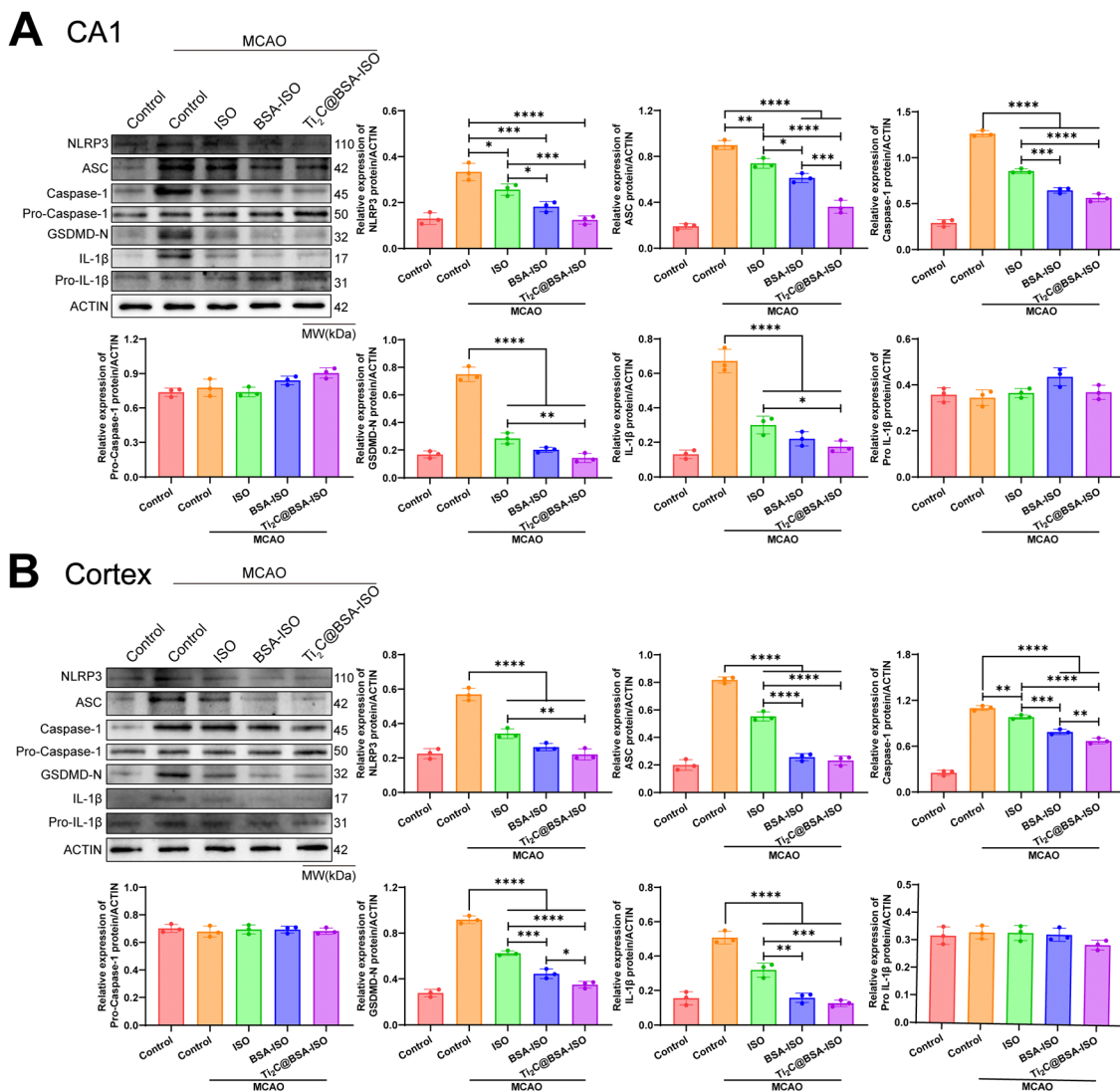
2802 | *J. Mater. Chem. B*, 2024, **12**, 2795–2806

This journal is © The Royal Society of Chemistry 2024

Fig. 7 Ti$_2$C@BSA-ISO inhibits the NLRP3/caspase-1/GSDMD pathway-mediated microglia pyroptosis. Representative western blot results of pyroptosis-related proteins were shown, along with quantitative analysis of NLRP3, ASC, pro-caspase-1, caspase-1, GSDMD-N, pro-IL-1β, and IL-1β in (A) hippocampal CA1 region and (B) cerebral cortex.

hippocampal CA1 region and cerebral cortex, after MCAO. Next, we evaluated the impact of BSA@ISO on pyroptosis following MCAO. In both the hippocampal CA1 region and cerebral cortex, Ti$_2$C@BSA-ISO treatment was able to significantly reduce the proportion of cleaved caspase-1 and NLRP3-positive cells compared to the BSA@ISO and ISO groups (Fig. 6A and B). Meanwhile, Ti$_2$C@BSA-ISO treatment reduced the levels of pyroptosis-related proteins, such as NLRP3, ASC, cleaved caspase-1, GSDMD-N, and IL-1β (Fig. 7A and B). In summary, Ti$_2$C@BSA-ISO significantly alleviated the ischemic stroke after MCAO by suppressing the NLRP3/caspase-1/GSDMD pathway-mediated pyroptosis in the rat hippocampal CA1 region and cerebral cortex.

Thrombolysis and neuroprotection are two current major therapeutic strategies to overcome ischemic and reperfusion damage. Recombinant tissue-type fibrinogen activator (tPA) is the only thrombolytic drug approved by the US Food and Drug Administration (FDA).[56] However, it has been shown that tPA

does not provide durable protection for ischemic stroke patients, possibly due to its short half-life in plasma.[57] In addition, thrombolytic therapy alone cannot block the large amount of ROS generated by reperfusion, which may cause secondary injury and lead to poor prognosis. Antioxidant nanomaterials are capable of controlling ROS levels under pathological conditions, eliminating ROS in ischemia–reperfusion tissues, and mitigating tissue and cell damage in ischemic stroke animal models.[24] MXene has attracted considerable attention for its potential biomedical applications due to its controllable catalytic properties and physicochemical characteristics.[58] In terms of antioxidants, suitable MXene candidates with multiple enzyme-mimicking properties and excellent antioxidant capacity can catalyse toxic/harmful molecules into non-toxic water and oxygen molecules, significantly inhibiting the elevation of ROS. By scavenging ROS to exert neuroprotective effects on ischemic stroke, MXene nanoenzymes such as Ti$_3$C$_2$, Ti$_2$C, and V$_2$C have therapeutic potential

This journal is © The Royal Society of Chemistry 2024

J. Mater. Chem. B, 2024, **12**, 2795–2806 | **2803**

for the treatment of ischemic stroke as well as other disorders with imbalanced redox homeostasis.[42,43] In addition, the large specific area and multiple surface groups of MXenes endow them with high drug-carrying capacity.[59] In this study, Ti_2C acted as an antioxidant to protect the neuronal cells and on the other hand acted synergistically as a carrier of the free radical scavenger ISO. Specifically, hydrophobic ISO was encapsulated in BSA and then modified on the surface of Ti_2C to form Ti_2C@BSA-ISO. The enzyme-mimicking activity of Ti_2C endowed Ti_2C@BSA-ISO with antioxidant capacity to reverse ROS-induced cell death, thereby protecting neural cells. *In vivo*, Ti_2C@BSA-ISO promoted neuroprotection and ROS scavenging in the hippocampal CA1 region and cerebral cortex of rats to alleviate ischaemic stroke. Ti_2C@BSA-ISO has acceptable therapeutic results compared to previous studies.[24,43,60] The long-held belief that titanium is inert and safe for human use can be seen as one of the main reasons for using titanium as an implant.[61] Compared to other elements (Mn, Cu), Ti_2C@BSA-ISO has a safe composition and has a broader scope for disease treatment. Interestingly, Ti_2C@BSA-ISO alleviated ischemic stroke by inhibiting NLRP3/caspase-1/GSDMD pathway-mediated pyroptosis. This contributes to the understanding of the interactions and signalling pathways between nanomaterials and pyroptosis and is important for nanomaterial targetedpyroptosis to treat diseases.

3. Conclusions

In conclusion, we successfully prepared a nanoformulation for the treatment of ischemic stroke. The formulation utilized Ti_2C nanoenzyme as a carrier, BSA-encapsulated hydrophobic drug isoquercetin (BSA-ISO) as a payload, and exhibited strong free radical scavenging ability. The experimental results showed that Ti_2C@BSA-ISO alleviated ischemic stroke by promoting neuroprotection and scavenging ROS to inhibit the pyroptosis of the rat hippocampal CA1 region and the cerebral cortex. Therefore, this study extends the neuroprotective and antioxidant-pyroptosis mechanisms of MXene surface nanoengineering, providing a new avenue for treating ischemic stroke.

Abbreviations

ISO	Isoquercitrin
MCAO	Middle cerebral artery occlusion
ROS	Reactive oxygen species
SOD	Superoxide dismutase
CAT	Catalase
GPx	Glutathione peroxidase
NLRP3	NOD-like receptor thermal protein domain associated protein 3
ASC	Apoptosis speck-like protein containing a caspase recruitment domain
Caspase-1	Cysteinyl aspartate specific proteinase-1
GSDMD-N	N-terminal Gasdermin-D
IL-1β	Interleukin-1β

Author contributions

Limin Fan: design, methodology, investigation, formal analysis, manuscript preparation. Xinhua Lin: methodology, investigation, manuscript preparation, and editing. Limin Hong: methodology, investigation, manuscript preparation and editing. Lehui Li and Run Lin: methodology, formal analysis in characterization. Tianbin Ren: resources, funding acquisition. Ji Tian and Miao Chen: conceptualization, design, methodology, resources, writing original draft, supervision, funding acquisition. All authors reviewed the manuscript.

Conflicts of interest

The authors report no conflicts of interest in this work.

Acknowledgements

References

1 S. K. Feske, *Am. J. Med.*, 2021, **134**, 1457–1464.
2 E. J. Benjamin, P. Muntner, A. Alonso, M. S. Bittencourt, C. W. Callaway, A. P. Carson, A. M. Chamberlain, A. R. Chang, S. Cheng, S. R. Das, F. N. Delling, L. Djousse, M. S. V. Elkind, J. F. Ferguson, M. Fornage, L. C. Jordan, S. S. Khan, B. M. Kissela, K. L. Knutson, T. W. Kwan, D. T. Lackland, T. T. Lewis, J. H. Lichtman, C. T. Longenecker, M. S. Loop, P. L. Lutsey, S. S. Martin, K. Matsushita, A. E. Moran, M. E. Mussolino, M. O'Flaherty, A. Pandey, A. M. Perak, W. D. Rosamond, G. A. Roth, U. K. A. Sampson, G. M. Satou, E. B. Schroeder, S. H. Shah, N. L. Spartano, A. Stokes, D. L. Tirschwell, C. W. Tsao, M. P. Turakhia, L. B. VanWagner, J. T. Wilkins, S. S. Wong, S. S. Virani, A. H. A. C. Epid, P. S. Comm and S. S. Subcomm, *Circulation*, 2019, **139**, E56–E528.
3 X. Y. Liu, M. Yang, F. Lei, Y. R. Wang, M. Y. Yang and C. B. Mao, *Adv. Mater.*, 2022, **34**, e2201210.
4 J. Liao, Y. Li, Y. C. Luo, S. Meng, C. Zhang, L. Y. Xiong, T. F. Wang and Y. Lu, *Mol. Pharmaceutics*, 2022, **19**, 3026–3041.
5 E. H. Lo, T. Dalkara and M. A. Moskowitz, *Nat. Rev. Neurosci.*, 2003, **4**, 399–415.
6 X. Li, Z. Han, T. Wang, C. Ma, H. Li, H. Lei, Y. Yang, Y. Wang, Z. Pei, Z. Liu, L. Cheng and G. Chen, *Biomaterials*, 2022, **291**, 121904.
7 E. E. Chouchani, V. Pell, E. Gaude, D. Aksentijevic, S. Sundier, M. Duchen, M. Shattock, C. Frezza, T. Krieg, M. Murphy, M. R. C. Uk, C. I. H. Res, G. C. Trust and B. H. Fdn, *Eur. J. Heart Failure*, 2015, **17**, 29–30.

2804 | *J. Mater. Chem. B*, 2024, **12**, 2795–2806

This journal is © The Royal Society of Chemistry 2024

8 S. S. Andrabi, S. Parvez and H. Tabassum, *Protoplasma*, 2020, **257**, 335–343.

9 A. Chamorro, U. Dirnagl, X. Urra and A. M. Planas, *Lancet Neurol.*, 2016, **15**, 869–881.

10 D. Jiang, D. Ni, Z. T. Rosenkrans, P. Huang, X. Yan and W. Cai, *Chem. Soc. Rev.*, 2019, **48**, 3683–3704.

11 K. Fan, J. Xi, L. Fan, P. Wang, C. Zhu, Y. Tang, X. Xu, M. Liang, B. Jiang, X. Yan and L. Gao, *Nat. Commun.*, 2018, **9**, 1440.

12 K. M. Holmstrom and T. Finkel, *Nat. Rev. Mol. Cell Biol.*, 2014, **15**, 411–421.

13 X. Zhao, L. Y. Wang, J. M. Li, L. M. Peng, C. Y. Tang, X. J. Zha, K. Ke, M. B. Yang, B. H. Su and W. Yang, *Adv. Sci.*, 2021, **8**, e2101498.

14 B. Poljsak, D. Suput and I. Milisav, *Oxid. Med. Cell. Longevity*, 2013, **2013**, 956792.

15 Y. L. Liu and J. J. Shi, *Nano Today*, 2019, **27**, 146–177.

16 X. Li, Z. H. Han, T. Y. Wang, C. Ma, H. Y. Li, H. L. Lei, Y. Q. Yang, Y. J. Wang, Z. F. Pei, Z. Liu, L. Cheng and G. Chen, *Biomaterials*, 2022, **291**, 121904.

17 M. Soh, D. W. Kang, H. G. Jeong, D. Kim, D. Y. Kim, W. Yang, C. Song, S. Baik, I. Y. Choi, S. K. Ki, H. J. Kwon, T. Kim, C. K. Kim, S. H. Lee and T. Hyeon, *Angew. Chem., Int. Ed.*, 2017, **56**, 11399–11403.

18 A. Gupta, S. Das, C. J. Neal and S. Seal, *J. Mater. Chem. B*, 2016, **4**, 3195–3202.

19 S. Fernandez-Garcia, L. Jiang, M. Tinoco, A. B. Hungria, J. Han, G. Blanco, J. J. Calvino and X. W. Chen, *J. Phys. Chem. C*, 2016, **120**, 1891–1901.

20 H. Wei and E. K. Wang, *Chem. Soc. Rev.*, 2013, **42**, 6060–6093.

21 W. Li, Z. Liu, C. Q. Liu, Y. J. Guan, J. S. Ren and X. G. Qu, *Angew. Chem., Int. Ed.*, 2017, **56**, 13661–13665.

22 N. Singh, M. A. Savanur, S. Srivastava, P. D'Silva and G. Mugesh, *Angew. Chem., Int. Ed.*, 2017, **56**, 14267–14271.

23 J. Wang, Y. Wang, X. Xiaohalati, Q. F. Su, J. W. Liu, B. Cai, W. Yang, Z. Wang and L. Wang, *Adv. Sci.*, 2023, **10**, e2206854.

24 Z. R. Wang, Y. Zhao, Y. X. Hou, G. H. Tang, R. F. Zhang, Y. L. Yang, X. Y. Yan and K. L. Fan, *Adv. Mater.*, 2023, e2210144.

25 J. Shan, X. Liu, X. Li, Y. Yu, B. Kong and L. Ren, *Eng. Regener.*, 2023, **4**, 95–102.

26 J. Pang, R. G. Mendes, A. Bachmatiuk, L. Zhao, H. Q. Ta, T. Gemming, H. Liu, Z. Liu and M. H. Rummeli, *Chem. Soc. Rev.*, 2019, **48**, 72–133.

27 Y. Sun, S. Gao, F. Lei, C. Xiao and Y. Xie, *Acc. Chem. Res.*, 2015, **48**, 3–12.

28 Y. Chen, C. Tan, H. Zhang and L. Wang, *Chem. Soc. Rev.*, 2015, **44**, 2681–2701.

29 D. Yim, D. E. Lee, Y. So, C. Choi, W. Son, K. Jang, C. S. Yang and J. H. Kim, *ACS Nano*, 2020, **14**, 10324–10336.

30 S. Syama and P. V. Mohanan, *Nano-Micro Lett.*, 2019, **11**, 6.

31 X. Y. Zhang, X. Nan, W. Shi, Y. N. Sun, H. L. Su, Y. He, X. Liu, Z. Zhang and D. T. Ge, *Nanotechnology*, 2017, **28**, 295102.

32 S. K. Lim, P. Chen, F. L. Lee, S. Moochha and B. Liedberg, *Anal. Chem.*, 2015, **87**, 9408–9412.

33 C. S. Wang, J. Y. Li, C. Amatore, Y. Chen, H. Jiang and X. M. Wang, *Angew. Chem., Int. Ed.*, 2011, **50**, 11644–11648.

34 S. B. Liu, T. H. Zeng, M. Hofmann, E. Burcombe, J. Wei, R. R. Jiang, J. Kong and Y. Chen, *ACS Nano*, 2011, **5**, 6971–6980.

35 J. Y. Gou, L. Zhao, Y. Li and J. Z. Zhang, *ACS Appl. Nano Mater.*, 2021, **4**, 12308–12315.

36 J. Y. Gou, L. Zhao, Y. Li and J. Z. Zhang, *ACS Appl. Nano Mater.*, 2021, **4**, 12308–12315.

37 C. F. J. Zhang, S. Pinilla, N. McEyoy, C. P. Cullen, B. Anasori, E. Long, S. H. Park, A. Seral-Ascaso, A. Shmeliov, D. Krishnan, C. Morant, X. H. Liu, G. S. Duesberg, Y. Gogotsi and V. Nicolosi, *Chem. Mater.*, 2017, **29**, 4848–4856.

38 V. Kumar, S. K. Shukla, M. Choudhary, J. Gupta, P. Chaudhary, S. Srivastava, M. Kumar, M. Kumar, D. K. Sarma, B. C. Yadav and V. Verma, *Sensors*, 2022, **22**, 5589.

39 B. Ahmed, D. H. Anjum, M. N. Hedhili, Y. Gogotsi and H. N. Alshareef, *Nanoscale*, 2016, **8**, 7580–7587.

40 A. Ghosh, S. Sarkar, A. K. Mandal and N. Das, *PLoS One*, 2013, **8**, e57735.

41 D. J. Park, F. A. Shah and P. O. Koh, *J. Vet. Med. Sci.*, 2018, **80**, 676–683.

42 W. Feng, X. G. Han, H. Hu, M. Q. Chang, L. Ding, H. J. Xiang, Y. Chen and Y. H. Li, *Nat. Commun.*, 2021, **12**, 2203.

43 H. Hu, H. Huang, L. L. Xia, X. Q. Qian, W. Feng, Y. Chen and Y. H. Li, *Chem. Eng. J.*, 2022, **440**, 135810.

44 J. Barrington, E. Lemarchand and S. M. Allan, *Brain Pathol.*, 2017, **27**, 205–212.

45 Z. F. Dong, K. Pan, J. R. Pan, Q. X. Peng and Y. D. Wang, *Neurosci. Bull.*, 2018, **34**, 1131–1136.

46 J. J. Shi, Y. Zhao, K. Wang, X. Y. Shi, Y. Wang, H. W. Huang, Y. H. Zhuang, T. Cai, F. C. Wang and F. Shao, *Nature*, 2015, **526**, 660–665.

47 S. Y. Kuang, J. Zheng, H. Yang, S. H. Li, S. Y. Duan, Y. F. Shen, C. N. Ji, J. H. Gan, X. W. Xu and J. X. Li, *Proc. Natl. Acad. Sci. U. S. A.*, 2017, **114**, 10642–10647.

48 L. B. Sun, W. Ma, W. L. Gao, Y. M. Xing, L. X. Chen, Z. Y. Xia, Z. J. Zhang and Z. L. Dai, *Cell Death Dis.*, 2019, **10**, 542.

49 Y. J. Luo, C. Reis and S. Chen, *Curr. Neuropharmacol.*, 2019, **17**, 582–589.

50 S. Singh and S. Jha, *Mol. Neurobiol.*, 2018, **55**, 8154–8178.

51 L. Minutoli, D. Puzzolo, M. Rinaldi, N. Irrera, H. Marini, V. Arcoraci, A. Bitto, G. Crea, A. Pisani, F. Squadrito, V. Trichilo, D. Bruschetta, A. Micali and D. Altavilla, *Oxid. Med. Cell. Longevity*, 2016, **2016**, 2183026.

52 X. Wei, F. Xie, X. X. Zhou, Y. C. Wu, H. Y. Yan, T. Liu, J. Huang, F. W. Wang, F. F. Zhou and L. Zhang, *Cell. Mol. Immunol.*, 2022, **19**, 971–992.

53 P. F. Xu, Y. Hong, Y. Xie, K. Yuan, J. J. Li, R. Sun, X. H. Zhang, X. L. Shi, R. R. Li, J. N. Wu, X. F. Liu, W. Hu and W. Sun, *Transl. Stroke Res.*, 2021, **12**, 643–659.

54 J. Hu, C. Zeng, J. Wei, F. Q. Duan, S. J. Liu, Y. H. Zhao and H. M. Tan, *Phytomedicine*, 2020, **76**, 153251.

55 M. K. Mamik and C. Power, *Brain*, 2017, **140**, 2273–2285.

This journal is © The Royal Society of Chemistry 2024

J. Mater. Chem. B, 2024, **12**, 2795–2806 | **2805**

56 F. Fluri, M. K. Schuhmann and C. Kleinschnitz, *Drug Des., Dev. Ther.*, 2015, **9**, 3445–3454.

57 W. B. Zhu, N. L. Libal, A. Casper, S. Bodhankar, H. Offner and N. J. Alkayed, *Transl. Stroke Res.*, 2014, **5**, 612–617.

58 S. Iravani and R. S. Varma, *Nano-Micro Lett.*, 2022, **14**, 213.

59 L. Li, Y. Lu, Z. T. Qian, Z. Y. Yang, S. F. Zong, Z. Y. Wang and Y. P. Cui, *Nanoscale*, 2021, **13**, 18546–18557.

60 J. Kong, R. Zou, R. Chu, N. Hu, J. Liu, Y. Sun, X. Ge, M. Mao, H. Yu and Y. Wang, *ACS Nano*, 2023, **18**, 4140–4158.

61 M. Kaur and K. Singh, *Mater. Sci. Eng., C*, 2019, **102**, 844–862.

2806 | *J. Mater. Chem. B*, 2024, **12**, 2795–2806

This journal is © The Royal Society of Chemistry 2024